HHS Public Access

Author manuscript

Neuroimage. Author manuscript; available in PMC 2023 February 01.

Published in final edited form as:

Neuroimage. 2023 February 01; 266: 119829. doi:10.1016/j.neuroimage.2022.119829.

MRI assessment of cerebral oxygen extraction fraction in the medial temporal lobe

Dengrong Jiang[a,*], **Peiying Liu**[a], **Zixuan Lin**[a], **Kaisha Hazel**[a], **George Pottanat**[a], **Emma Lucke**[b], **Abhay Moghekar**[c], **Jay J. Pillai**[a,d], **Hanzhang Lu**[a,e,f]

[a]The Russell H. Morgan Department of Radiology & Radiological Science, Johns Hopkins University School of Medicine, Baltimore, MD, United States

[b]Department of Biology, Johns Hopkins University School of Arts & Sciences, Baltimore, MD, United States

[c]Department of Neurology, Johns Hopkins University School of Medicine, Baltimore, MD, United States

[d]Department of Neurosurgery, Johns Hopkins University School of Medicine, Baltimore, MD, United States

[e]Department of Biomedical Engineering, Johns Hopkins University School of Medicine, Baltimore, MD, United States

[f]F. M. Kirby Research Center for Functional Brain Imaging, Kennedy Krieger Research Institute, Baltimore, MD, United States

Abstract

The medial temporal lobe (MTL) is a key area implicated in many brain diseases, such as Alzheimer's disease. As a functional biomarker, the oxygen extraction fraction (OEF) of MTL may be more sensitive than structural atrophy of MTL, especially at the early stages of diseases. However, there is a lack of non-invasive techniques to measure MTL-OEF in humans. The goal of this work is to develop an MRI technique to assess MTL-OEF in a clinically practical time without using contrast agents. The proposed method measures venous oxygenation ($Y_{v)}$ in the basal veins of Rosenthal (BVs), which are the major draining veins of the MTL. MTL-OEF can then be estimated as the arterio-venous difference in oxygenation. We developed an

*Corresponding author. djiang9@jhmi.edu (D. Jiang).

Declaration of Competing Interest

The authors have no competing interests or financial disclosures to report.

Credit authorship contribution statement

Dengrong Jiang: Conceptualization, Methodology, Software, Formal analysis, Investigation, Writing – original draft, Visualization. **Peiying Liu:** Conceptualization, Methodology, Investigation, Writing – review & editing, Funding acquisition. **Zixuan Lin:** Methodology, Software, Writing – review & editing. **Kaisha Hazel:** Investigation, Resources, Data curation, Writing – review & editing. **George Pottanat:** Investigation, Resources, Data curation, Writing – review & editing. **Emma Lucke:** Data curation, Writing – review & editing. **Abhay Moghekar:** Conceptualization, Resources, Writing – review & editing. **Jay J. Pillai:** Conceptualization, Methodology, Writing – review & editing. **Hanzhang Lu:** Conceptualization, Methodology, Investigation, Resources, Writing – review & editing, Supervision, Project administration, Funding acquisition.

Supplementary materials

Supplementary material associated with this article can be found, in the online version, at doi:10.1016/j.neuroimage.2022.119829.

MRI sequence, dubbed arterial-suppressed accelerated T_2-relaxation-under-phase-contrast (AS-aTRUPC), to quantify the blood T_2 of the BVs, which was then converted to Y_v through a well-established calibration model. MTL-OEF was calculated as $(Y_a - Y_v)/Y_a \times 100\%$, where Y_a was the arterial oxygenation. The feasibility of AS-aTRUPC to quantify MTL-OEF was evaluated in 16 healthy adults. The sensitivity of AS-aTRUPC in detecting OEF changes was assessed by a caffeine ingestion (200 mg) challenge. For comparison, T_2-relaxation-under-spin-tagging (TRUST) MRI, which is a widely used global OEF technique, was also acquired. The dependence of MTL-OEF on age was examined by including another seven healthy elderly subjects. The results showed that in healthy adults, MTL-OEF of the left and right hemispheres were correlated ($P = 0.005$). MTL-OEF was measured to be 23.9 ± 3.6% (mean ± standard deviation) and was significantly lower ($P < 0.0001$) than the OEF of 33.3 ± 2.9% measured in superior sagittal sinus (SSS). After caffeine ingestion, there was an absolute percentage increase of 9.1 ± 4.0% in MTL-OEF. Additionally, OEF in SSS measured with AS-aTRUPC showed a strong correlation with TRUST OEF (intra-class correlation coefficient = 0.94 with 95% confidence interval [0.91, 0.96]), with no significant bias ($P = 0.12$). MTL-OEF was found to increase with age (MTL-OEF = 20.997 + 0.100 × age; $P = 0.02$). In conclusion, AS-aTRUPC MRI provides non-invasive assessments of MTL-OEF and may facilitate future clinical applications of MTL-OEF as a disease biomarker.

Keywords

Oxygen extraction fraction; Medial temporal lobe; Basal vein of Rosenthal; Venous oxygenation; Aging; Alzheimer's disease

1. Introduction

The medial temporal lobe (MTL), including the hippocampus, is crucial for memory formation and is implicated in many brain diseases (Blumcke et al., 2013; Burton et al., 2009; Jack et al., 1997; Mathew et al., 2014; Ohnishi et al., 2000). For example, MTL atrophy is a known hallmark of Alzheimer's disease (Burton et al., 2009; Jack et al., 1997) and medial temporal sclerosis, which is a major cause of adult epilepsy (Blumcke et al., 2013). However, structural atrophy represents a late stage of MTL dysfunction and is generally considered irreversible. On the other hand, neurofunctional assessment of the MTL may provide a sensitive biomarker in the early stages of brain diseases. Since neural activity is tightly coupled to the brain's oxygen consumption (Attwell and Laughlin, 2001), oxygen extraction fraction (OEF) in the MTL (MTL-OEF) has great potential in the diagnosis and treatment monitoring of neurological and psychiatric diseases (Ishii et al., 1996).

Measurement of MTL-OEF is highly challenging. PET with ^{15}O-labeled radiotracers is widely regarded as the gold-standard for OEF mapping (Mintun et al., 1984). An early ^{15}O-PET study showed that patients with Alzheimer's disease had lower MTL-OEF than healthy controls (Ishii et al., 1996). However, the ^{15}O-PET method involves ionizing radiation, requires dynamic sampling of arterial blood for input function estimation, and needs an onsite cyclotron to produce the ^{15}O isotope (half-life ~2 minutes). Therefore, these complexities have limited the availability of ^{15}O-PET imaging.

The MRI signal is sensitive to OEF, an example of which is the well-known blood-oxygenation-level-dependent (BOLD) MRI (Hoge et al., 1999). In the past decades, several MRI methods have been proposed to quantify OEF (An and Lin, 2003; Bulte et al., 2012; Cho et al., 2018; Fan et al., 2014; Haacke et al., 2010; Jain et al., 2010; Wise et al., 2013). However, measurement of MTL-OEF has not been reported. OEF can be quantified as the arterio-venous difference in oxygenation. In this relationship, arterial oxygenation is relatively constant (~98% or can be easily measured with pulse oximetry). Therefore, the main challenge lies in the measurement of venous oxygenation (Y_v). Based on the human venous anatomy, major MTL structures including hippocampus, parahip-pocampal gyrus and amygdala, are primarily drained by the basal veins of Rosenthal (BVs) (Fig. 1 A), although a small fraction of MTL may be drained by other veins such as the cavernous sinus or internal cerebral veins (Fernandez-Miranda et al., 2010; Xu et al., 2021). BVs have relatively few variations across individuals (Rhoton, 2002; Tubbs et al., 2007). Therefore, the present work aims to develop an MRI technique to specifically measure Y_v in the BVs, from which MTL-OEF was estimated. The sensitivity of the technique in detecting OEF changes was assessed with a vasoactive caffeine challenge. Finally, we examined the change of MTL-OEF with normal aging.

2. Materials and methods

2.1. MRI pulse sequence

We propose an arterial-suppressed accelerated T_2-relaxation-under-phase-contrast (AS-aTRUPC) MRI sequence to measure the oxygenation in the BVs. It is based on the principle that blood T_2 has a well-known and calibratable relationship with blood oxygenation (Lu et al., 2012; van Zijl et al., 1998). Briefly, this sequence utilizes phase-contrast (Fig. 1 B, green boxes) complex subtraction to isolate pure blood signals from brain tissues. T_2 of the blood signal can then be quantified by using T_2 -preparation (Fig. 1 B, red box) with varying effective echo times (eTEs) to modulate the T_2 -weighting. At each eTE, three sets of images, specifically phase reference images, anterior-posterior flow-encoded images, and right-left flow-encoded images, are acquired in an interleaved manner. For the flow-encoded images, bipolar gradients (Fig. 1 B, green box) are applied to modulate the phase of the spins such that blood spins flowing along a certain direction (e.g., anterior-posterior) accumulate a phase while the static tissue spins do not accrue any phase. In this work, we used two flow-encoding directions because the BVs tend to run obliquely from anterior-lateral to posterior-medial direction. In contrast, the phase reference images are flow-compensated, i.e., neither blood nor static tissue spins accumulate any phase. Therefore, complex subtraction between phase reference and flow-encoded images cancels out the static tissue signals and leaves only the flowing blood signals in the vessels, which eliminates the partial volume effects (Bernstein et al., 2004). The T_2-preparation module uses non-selective composite refocusing pulses to allow robust T_2 estimation that is insensitive to flow or magnetic field inhomogeneity (Brittain et al., 1995). Once blood T_2 is obtained, it can be converted to Y_v through a calibration model (Lu et al., 2012). Finally, OEF can be calculated as the arterio-venous difference in oxygenation.

To differentiate BVs from the posterior cerebral arteries that are anatomically adjacent to the veins, a series of arterial-suppression pulses (Fig. 1 B, black boxes) are played before T_2-preparation. In addition, one arterial-suppression pulse is applied before each phase-contrast acquisition module. This is to ensure that the incoming arterial blood is suppressed throughout the acquisition train. To reduce the scan time, a turbo field echo (TFE) scheme with variable flip-angles is employed to acquire multiple *k* space lines per repetition time (TR) (Jiang et al., 2019). After the acquisition train, post-saturation pulses (Fig. 1 B, blue box) are applied to reset the spin history.

2.2. Scan procedures

Fig. 2 A shows the general scan procedures to assess MTL-OEF. First, to visualize the BVs, a time of flight (TOF) venogram was acquired. The venogram was placed coronally and covered the middle part of the brain (Fig. 2 B). The preliminary slice orientation and location of the AS-aTRUPC scan were determined based on the venogram. Next, to refine the location of AS-aTRUPC to cover bilateral BVs in the same slice, an axial 3D susceptibility weighted imaging (SWI) scan was performed and minimum intensity projection images were generated in a sliding window manner. Finally, we positioned the imaging slice of AS-aTRUPC at the location where the SWI minimum intensity projection image showed the best coverage of the bilateral BVs, and performed the AS-aTRUPC sequence. The arterial-suppression slab was placed 10mm below the imaging slice (Fig. 2 B).

2.3. General experimental method

The study protocol was approved by the Johns Hopkins University Institutional Review Board and written informed consent was obtained from each participant. All participants were healthy based on self-report, and were recruited from January 2021 to April 2022. All MRI experiments were performed on a 3T Prisma scanner (Siemens Healthcare, Erlangen, Germany), using the body coil for transmission and a 32-channel head coil for receiving.

2.4. Study 1: Technical study

Sixteen healthy adults (mean age ± standard deviation, 29.3 ± 7.7 years, 9 females and 7 males) were scanned following the procedures described in Section 2.2.

The TOF venogram used the following parameters: 2D, field of view (FoV) = 200 × 200mm^2, slice thickness = 2mm, in-plane resolution = 0.78 × 0.78mm^2, 48 slices, TR = 28ms, echo time (TE) = 7ms and scan time = 2.7min.

The parameters of SWI were: 3D, FoV = 180 × 220 × 50mm^3, voxel-size = 0.94 × 0.94 × 1.25mm^3, TR = 30ms, TE = 24ms, scan time = 2.2min.

AS-aTRUPC used the following parameters: 2D, single slice, FoV = 200 × 200mm^2, slice thickness = 10mm, reconstructed in-plane resolution = 0.78 × 0.78mm^2, recovery time = 1000ms, TFE factor = 15, GRAPPA factor = 2, velocity-encoding (VENC) = 7cm/s with two directions (anterior-posterior and right-left), arterial-suppression slab thickness = 40mm

with a gap of 10mm below the imaging slice, 3 eTEs: 0, 40 and 80ms, 4 averages, total scan time = 4.8min.

2.5. Study 2: Caffeine challenge

To evaluate the sensitivity of AS-aTRUPC in detecting OEF changes, in a subset of ten subjects (26.0 ± 3.9 years, 6 females and 4 males), we conducted a caffeine challenge, which is known to reduce cerebral blood flow (CBF) (Addicott et al., 2009) and increase OEF (Xu et al., 2015).

For comparison with AS-aTRUPC, we also measured global cortical OEF in the superior sagittal sinus (SSS) using a well-established technique, T_2-relaxation-under-spin-tagging (TRUST) MRI, which has been validated against gold-standard ^{15}O-PET (Jiang et al., 2021). The TRUST sequence parameters followed recent reports (Jiang et al., 2021; Jiang et al., 2018): 2D single slice, single-shot echo planar imaging readout, FoV = 220 × 220mm^2, slice thickness = 5mm, in-plane resolution = 3.44 × 3.44mm^2, TR = 3000ms, TE = 4ms, inversion time = 1020ms, 4 eTEs:0, 40, 80, and 160ms, 3 dynamics, scan time = 1.2min.

The experimental procedures are listed in Fig. 3. TOF, SWI and AS-aTRUPC used the same parameters as described in Study 1. Each subject first underwent one TRUST and one AS-aTRUPC scan to measure baseline OEF values. Then the participant was taken out of the scanner, sat up on the table, ingested a 200mg caffeine tablet (Sunmark, McKesson Brand, Irving, TX) (equivalent to 2 cups of regular coffee) and was quickly put back into the scanner. The participant then underwent another 8 TRUST and AS-aTRUPC scans to assess the caffeine-induced OEF changes.

2.6. Study 3: Aging effect

To examine the aging effect on MTL-OEF, we scanned another seven healthy older subjects (65.9 ± 12.0 years, 4 females and 3 males) using the same scan procedures as in Study 1. Data of these seven subjects were pooled with those of the sixteen younger subjects in Study 1 to evaluate the association of MTL-OEF with age. The age range of the total 23 subjects was from 19 to 81 years old.

2.7. Data processing

2.7.1. AS-aTRUPC data processing—The AS-aTRUPC data were processed using in-house MATLAB (Math-works, Natick, MA) scripts. Phase artifacts induced by Maxwell concomitant field and eddy currents were corrected using a hyperplane fitting method (Bernstein et al., 1998; Krishnamurthy et al., 2016). Motion correction among images was performed using the Statistical Parametric Mapping 12 tool (SPM12, University College London, London, UK).

For each eTE, a complex-difference (CD) image was obtained by complex subtraction between the phase reference image and the flow-encoded image. This procedure was repeated for anterior-posterior and right-left flow-encoded data, resulting in CD_{AP} and CD_{RL}, as illustrated √ calculated in Fig. 4 A. A combined vessel image CD_{comb} was as $\sqrt{|CD_{AP}|^2 + |CD_{RL}|^2}$. Four regions of interest (ROIs) were manually drawn on the eTE =

0ms CD_{comb} image: one on left BV, one on right BV, one on the vein of Galen (GV) and one on the SSS, as shown in Fig. 4 B. The BV ROIs were approximately 1cm in length and close to where the BVs emptied into the GV. Then, complex CD_{AP} and CD_{RL} signals inside each ROI were extracted and fitted as monoexponential functions of eTEs to yield the blood T_2. More details of the T_2 fitting method using complex signals are described in the Supplementary Material.

Because the T_2-preparation effect is dissipated later in the TFE acquisition train, the TFE T_2 measured by AS-aTRUPC is slightly different from standard T_2. To account for this bias, the AS-aTRUPC TFE T_2 was corrected using the following equation, which was determined in previous in-vivo human experiments (Jiang et al., 2019):

$$T_{2,\ \text{corrected}} = 1.2002 \times T_{2,\ \text{TFE}} - 10.6276 \quad (1)$$

where $T_{2,TFE}$ is the TFE T_2 estimated by AS-aTRUPC and $T_{2,corrected}$ is the corrected T_2. The Y_v of each ROI was converted from $T_{2,corrected}$ using a published calibration model (Lu et al., 2012), assuming a hematocrit level of 0.42 for males and 0.40 for females. Finally, OEF of each ROI was calculated by:

$$OEF = \frac{Y_a - Y_v}{Y_a} \times 100\% \quad (2)$$

where arterial oxygenation Y_a was assumed to be 98%.

2.7.2. TRUST data processing—The TRUST data were processed using in-house MATLAB scripts, following procedures in the literature (Jiang et al., 2021; Lu and Ge, 2008). Briefly, pair-wise subtraction between control and labeled images yielded difference images with pure venous blood signal in the SSS. An ROI encompassing the SSS was manually drawn on the eTE = 0ms difference image. The four voxels with the highest signal intensities within the ROI were selected as the final mask. The spatially averaged signals inside the final mask were fitted as a mono-exponential function of eTEs to yield blood T_2, which was converted to Y_v using the same calibration model as in AS-aTRUPC processing (Lu et al., 2012). Note that TRUST did not use TFE acquisition and therefore no T_2 correction was needed. Finally, TRUST OEF values were calculated using Equation 2.

2.8. Statistical analysis

All statistical analyses were performed using MATLAB. The normality of the OEF data was assessed using the Kolmogorov-Smirnov test. In Study 1, we first evaluated the correlation between OEF values of the left and right BVs in terms of intra-class correlation coefficient (ICC). Paired t-test was used to determine whether there was a significant difference in OEF values between the two sides. If the OEF values of left and right BVs were shown to be correlated and have no significant difference, then the averaged OEF of bilateral BVs was used to represent MTL-OEF. To examine whether there was a regional difference in OEF, one-way analysis-of-variance (ANOVA) followed by Tukey multiple comparison tests were used to compare the OEF values among BV, GV and SSS.

In Study 2, the dependence of OEF values on the time after caffeine ingestion was evaluated using mixed-effect models. We first tested a linear term of time to investigate whether OEF values in each vein changed over time. Then we further added a quadratic term of time to the models to evaluate whether the temporal change of OEF was non-linear. We also evaluated the correlation between AS-aTRUPC OEF and TRUST OEF (both measured at SSS) in terms of ICC. For this analysis, all the 9 scans (one baseline scan and eight scans after caffeine ingestion) of each of the ten subjects were included, yielding a total of 90 data points. Paired t-test was employed to determine whether there was a significant difference between AS-aTRUPC OEF and TRUST OEF.

In Study 3, to evaluate the aging effect on OEF, linear regression analyses were conducted using OEF values in each vein measured by AS-aTRUPC as the dependent variable and age as the independent variable. To examine the sex effect on OEF, two-sample t-tests assuming equal variance were used to compare the OEF values between males and females.

In all analyses, a two-tailed $P < 0.05$ was considered statistically significant.

3. Results

3.1. Study 1

Fig. 4 shows representative AS-aTRUPC data. Complex subtraction between the phase reference and the flow-encoded images (Fig. 4 A) yields CD images, in which the tissue signals are canceled out, leaving only the blood signal in the vessels (thereby eliminating partial volume effects). By combining the CD images of two flow-encoding directions (anterior-posterior and right-left), the full courses of BVs can be clearly seen. CD images at increasing T_2-weighting (i.e., eTEs) are shown in Fig. 4 B, including exemplary ROIs. Fitting of the CD signals as a function of eTEs is shown in Fig. 4 C.

The normality of the OEF values in each ROI was confirmed by Kolmogorov–Smirnov tests ($P > 0.05$). OEF values in the left and right BVs were significantly correlated (left OEF = 1.00 * right OEF, ICC = 0.65, $P = 0.005$, Fig. 5 A) and there was no difference between them (paired t-test $P = 0.94$, Fig. 5 B). The ratio of OEF in the left BV to OEF in the right BV was 1.00 ± 0.13. Therefore, the OEF values of bilateral BVs were averaged to represent MTL-OEF. Across the subjects, OEF in BVs, GV, and SSS were 23.9 ± 3.6% (mean ± standard deviation), 24.2 ± 3.9%, and 33.3 ± 2.9%, respectively (Fig. 5 C). One-way ANOVA revealed a significant difference in OEF values among the veins ($P < 0.0001$). Specifically, OEF in the BVs (which represents the MTL-OEF) was similar to OEF in the GV ($P = 0.98$), but both of them were lower than OEF in the SSS ($P < 0.0001$). Note that BVs empty into GV, both draining the deep brain structures. In contrast, SSS drains the superficial cortical tissues.

3.2. Study 2

Representative TRUST data is shown in Fig. S2. Fig. 6 A shows the time courses of OEF in different veins measured by AS-aTRUPC and TRUST. Table 1 summarizes the results of mixed-effect model analyses. When studying the linear relationship between OEF and time, we found that OEF increased after caffeine ingestion in all veins ($P < 0.0001$). Furthermore,

significant effects of the quadratic term, Time 2, were observed, suggesting that the OEF changes were non-linear with time. Comparing the last time point to baseline, the caffeine-induced absolute percentage increases in OEF were 9.1 ± 4.0%, 10.7 ± 3.8%, and 10.6 ± 2.9% in BVs, GV, and SSS, respectively. One-way ANOVA revealed no difference in the absolute percentage increases in OEF among the veins (P = 0.52). The extent of OEF increase in SSS was within the range reported in previous studies (Lin et al., 2022; Xu et al., 2015).

In addition, as shown in Fig. 6 B and 6 C, OEF in the SSS measured by AS-aTRUPC had a strong correlation with TRUST OEF, which was also assessed in the SSS (ICC = 0.94 with 95% confidence interval [0.91, 0.96]). No significant difference in OEF values was detected between the two techniques ($P = 0.12$).

3.3. Study 3

The results of linear regression analyses for the aging effect are summarized in Fig. 7 and Table 2. In the total 23 subjects (16 younger subjects and 7 older subjects), we found that MTL-OEF (i.e., OEF in BVs) increased with age ($P = 0.02$, Fig. 7 A) in that MTL-OEF = 20.997 + 0.100 × age. Age-related increase in OEF was also observed in the GV ($P = 0.002$, Fig. 7 B; GV-OEF = 19.741 + 0.146 × age) and in the SSS ($P = 0.001$, Fig. 7 C; SSS-OEF = 28.997 + 0.148 × age). OEF was not dependent on sex ($P > 0.5$ for all veins).

4. Discussion

This work represents the first report to quantitatively measure OEF in the BVs, which are the major veins draining the MTL. The measurement can be completed in less than 5 minutes without needing any contrast agents or ionizing radiation. We found that MTL-OEF was lower than the OEF in the superficial cortical tissues. In caffeine challenge studies, MTL-OEF showed a time-dependent increase, demonstrating the sensitivity of our technique in tracking OEF alterations. In the aging study, we observed that MTL-OEF increased with age, which to our knowledge is the first report of the age effect on MTL-OEF. MTL plays a critical role in human cognitive function, in particular memory formation. Therefore, the ability to measure MTL-OEF, an important parameter of the energy metabolism in the MTL, may provide a new functional biomarker in many brain diseases. In the present work, we observed a lower MTL-OEF compared to OEF in the superficial cortical tissues in healthy volunteers. Several ^{15}O-PET studies have also measured MTL-OEF in healthy subjects. For example, in fourteen healthy elderly subjects, Ishii et al. found that MTL-OEF was ~7 units (%) lower than OEF in other cortical regions (Ishii et al., 1996). Another three ^{15}O-PET studies reported that MTL-OEF was significantly lower than OEF in other cortical regions by 4–7 units (Hatazawa et al., 1995; Henriksen et al., 2021; Yamaguchi et al., 1986). Ibaraki et al. also showed lower MTL-OEF than OEF in other cortical regions in two ^{15}O-PET studies, although the authors did not perform statistical comparisons (Ibaraki et al., 2008; Ibaraki et al., 2009). Therefore, our observations using MRI were generally consistent with the existing ^{15}O-PET literature. The underlying causes of the lower OEF in the MTL merit further investigation. Some PET studies have reported that compared to neocortices, the MTL and other deep brain structures such as thalamus and basal ganglia, have a higher

ratio of CBF to the metabolic rate of glucose (Gur et al., 2009; Henriksen et al., 2018). This suggests hyper-perfusion in these regions relative to their energy demands, which may explain the lower OEF.

We observed that MTL-OEF increased with age. Age-related elevations of OEF were also found in superficial cortical tissues (drained by SSS) and other deep brain structures (drained by GV). Our data suggest that the OEF increase rate may vary among brain regions, in that OEF in SSS and GV seemed to increase faster with age compared to OEF in BVs (Table 2). While there is no prior report of the aging effect on MTL-OEF, our observation that OEF in the SSS increased with age was consistent with recent literature (Lu et al., 2011; Peng et al., 2014). Age-related increase in OEF may be attributed to two reasons. One is that CBF decreases with age (Chen et al., 2011; Lu et al., 2011; Peng et al., 2014). Thus, in order to extract sufficient oxygen for the brain's consumption, OEF has to be higher. The other possible reason is that there is some evidence suggesting that the brain's oxygen consumption rate is higher in older individuals (Lu et al., 2011; Peng et al., 2014) to compensate for the reduced cellular and computational efficiency. Thus, higher OEF is needed to support this elevated metabolic need.

Other MRI techniques have also been proposed to measure OEF of the brain (An and Lin, 2003; Bulte et al., 2012; Cho et al., 2018; Fan et al., 2014; Haacke et al., 2010; He and Yablonskiy, 2007; Jain et al., 2010; Lajoie et al., 2017; Wise et al., 2013). However, to date, none has been specifically applied to report OEF of the MTL. The phase-based oximetry method is limited to a whole-brain measure (Jain et al., 2010). The gas-inhalation method suffers from EPI-related image distortions in the MTL (Bulte et al., 2012; Lajoie et al., 2017; Wise et al., 2013). The quantitative BOLD method may be affected by the pronounced macroscopic susceptibility artifacts in the MTL region (An and Lin, 2003; Cho et al., 2018; He and Yablonskiy, 2007). The quantitative susceptibility mapping method is known to suffer from partial volume effects (Fan et al., 2014; Haacke et al., 2010) in small veins such as the BVs. The AS-aTRUPC technique proposed in this work takes less than 5 minutes and can be performed on a standard 3-Tesla MRI scanner without needing gas inhalation or contrast agent. Although the present work did not compare AS-aTRUPC MRI with ^{15}O-PET directly, we did study the relationship of AS-aTRUPC MRI with a PET-validated MRI technique, TRUST (Jiang et al., 2021). For the same region (i.e., SSS) measured with these two MRI techniques, their OEF revealed excellent agreement in terms of correlation and quantitative values. Therefore, AS-aTRUPC may facilitate wide clinical applications of MTL-OEF as a disease biomarker.

The estimation of MTL-OEF in this work is based on the notion that MTL is predominantly drained by the BVs. However, the BVs may also drain other nearby tissues such as insula, midbrain, part of the lateral ventricles and small portions of basal ganglia and thalami (Rhoton, 2002). Blood contribution from these regions could dilute the specificity of the MTL-OEF measurement, and may explain the observation that the MTL-OEF values measured in our study were slightly lower than those reported in the ^{15}O-PET literature. The exact proportion of BV blood that comes from the MTL is yet to be quantified in future studies (e.g., by measuring the blood flow rate in different segments of the BVs or their tributaries), and could be a confounding factor when applying our BV-based MTL-OEF

measurement to brain diseases such as Alzheimer's disease. However, we note that OEF, even measured at a global level, has been shown to be sensitive to Alzheimer's disease (Jiang et al., 2020; Lin et al., 2019; Thomas et al., 2017). Given the importance of MTL in Alzheimer's disease, OEF in the BVs, although not purely specific to the MTL, is expected to provide better sensitivity and specificity to Alzheimer's disease than global OEF. Compared to measuring OEF in smaller veins (such as the anterior longitudinal hippocampal vein which is a tributary of the BV) or at the tissue capillary level, quantifying OEF in the BVs has the advantages of relatively high signal-to-noise ratio and infrequent anatomical variations of the BVs (Rhoton, 2002; Tubbs et al., 2007). Therefore, we think BV-based MTL-OEF measurement represents a good tradeoff between regional specificity and technical sensitivity.

In the present work, we selected a VENC of 7cm/s in both anterior-posterior and right-left flow-encoding directions for AS-aTRUPC, because previous literature reported a flow velocity of 8–9cm/s in BVs and GV (MacDonald and Frayne, 2015; Mursch et al., 2001) and BVs tend to run in oblique directions from anterior-lateral to posterior-medial. Although the SSS has a faster flow velocity of 20–30cm/s (MacDonald and Frayne, 2015; Schuchardt et al., 2015), since the SSS was often at an angle of 80°−110° to the imaging plane (Fig. 2 B, yellow box), velocity components along the directions of the flow-encoding gradients (i.e., the cosine of the angle times the maximum velocity) were less than 10cm/s. Thus, our VENC of 7cm/s actually yielded substantial signal. More importantly, the AS-aTRUPC OEF measurement is based on the T_2 relaxation rate of the blood signal rather than the signal amplitude itself. Therefore, the quantification of OEF in the SSS should not be affected by the suboptimal VENC values and flow-encoding directions for SSS.

There are a few limitations in the present work. First, we only studied healthy adult volunteers, but have not applied the technique to patients with MTL abnormalities such as Alzheimer's disease and medial temporal sclerosis. These will be the goals of our future studies. Second, the hematocrit levels of the subjects were assumed (0.42 for males and 0.40 for females) rather than measured. It is known that men tend to have higher hematocrit than women and older adults may have lower hematocrit than young adults (Aanerud et al., 2012; Hawkins et al., 1954). Although we assumed a higher hematocrit value for males to account for the sex difference, we did not account for the decrease in hematocrit with age, which may confound our results on the age-related increase in OEF. We also assumed the deep veins such as BV and GV to have the same hematocrit as SSS, because a previous study showed that hematocrit in veins with a diameter > 70 μm are similar to systemic hematocrit (Lipowsky et al., 1980). Future studies are needed to verify whether deep veins have the same hematocrit as SSS. Third, we did not measure CBF (e.g., by using arterial spin labeling MRI) in the caffeine challenge study and were therefore unable to validate the relationship between the OEF increases in the veins and the caffeine-induced CBF reductions in the corresponding venous draining territories. Fourth, although the AS-aTRUPC sequence takes less than 5 minutes, in the present work, additional TOF and SWI scans were performed to localize the BVs, which added another 5 minutes to the whole scan procedure. However, we note that in clinical practice, sequences such as SWI are often included in the routine protocols for brain diseases. These routine sequences can also be used to localize the BVs for positioning AS-aTRUPC. Finally, although the AS-aTRUPC OEF values in general

showed an excellent agreement with PET-validated TRUST OEF measurements, slight biases can still be observed at the high and low ends of the OEF ranges, which merits further optimization of the AS-aTRUPC technique.

In conclusion, this work developed a novel MRI technique to estimate the oxygen extraction fraction of the medial temporal lobe in less than 5 minutes. This technique may be useful in studying brain diseases involving MTL dysfunction.

Supplementary Material

Refer to Web version on PubMed Central for supplementary material.

Acknowledgements

This work was supported by the National Institutes of Health under award numbers R01 AG064792, RF1 AG071515, R01 NS106711, R01 NS106702, R21 AG079098, UF1 NS100588, P41 EB031771, and RF1 NS110041.

Data and code availability statement

The data and code used in this work will be made available upon request on a case-by-case basis after obtaining approval from the funding agency.

References

Aanerud J, Borghammer P, Chakravarty MM, Vang K, Rodell AB, Jonsdottir KY, Moller A, Ashkanian M, Vafaee MS, Iversen P, Johannsen P, Gjedde A, 2012. Brain energy metabolism and blood flow differences in healthy aging. J. Cereb. Blood Flow Metab 32, 1177–1187. [PubMed: 22373642]

Addicott MA, Yang LL, Peiffer AM, Burnett LR, Burdette JH, Chen MY, Hayasaka S, Kraft RA, Maldjian JA, Laurienti PJ, 2009. The effect of daily caffeine use on cerebral blood flow: How much caffeine can we tolerate? Hum. Brain Mapp 30, 3102–3114. [PubMed: 19219847]

An H, Lin W, 2003. Impact of intravascular signal on quantitative measures of cerebral oxygen extraction and blood volume under normo- and hypercapnic conditions using an asymmetric spin echo approach. Magn. Reson. Med 50, 708–716. [PubMed: 14523956]

Attwell D, Laughlin SB, 2001. An energy budget for signaling in the grey matter of the brain. J. Cereb. Blood Flow Metab 21, 1133–1145. [PubMed: 11598490]

Bernstein MA, King KF, Zhou XJ, 2004. Handbook of MRI pulse sequences. Elsevier, pp. 659–678.

Bernstein MA, Zhou XJ, Polzin JA, King KF, Ganin A, Pelc NJ, Glover GH, 1998. Concomitant gradient terms in phase contrast MR: analysis and correction. Magn. Reson. Med 39, 300–308. [PubMed: 9469714]

Blumcke I, Thom M, Aronica E, Armstrong DD, Bartolomei F, Bernasconi A, Bernasconi N, Bien CG, Cendes F, Coras R, Cross JH, Jacques TS, Kahane P, Mathern GW, Miyata H, Moshe SL, Oz B, Ozkara C, Perucca E, Sisodiya S, Wiebe S, Spreafico R, 2013. International consensus classification of hippocampal sclerosis in temporal lobe epilepsy: a Task Force report from the ILAE Commission on Diagnostic Methods. Epilepsia 54, 1315–1329. [PubMed: 23692496]

Brittain JH, Hu BS, Wright GA, Meyer CH, Macovski A, Nishimura DG, 1995. Coronary angiography with magnetization-prepared T2 contrast. Magn. Reson. Med 33, 689–696. [PubMed: 7596274]

Bulte DP, Kelly M, Germuska M, Xie J, Chappell MA, Okell TW, Bright MG, Jezzard P, 2012. Quantitative measurement of cerebral physiology using respiratory-calibrated MRI. Neuroimage 60, 582–591. [PubMed: 22209811]

Burton EJ, Barber R, Mukaetova-Ladinska EB, Robson J, Perry RH, Jaros E, Kalaria RN, O'Brien JT, 2009. Medial temporal lobe atrophy on MRI differentiates Alzheimer's disease from dementia

with Lewy bodies and vascular cognitive impairment: a prospective study with pathological verification of diagnosis. Brain 132, 195–203. [PubMed: 19022858]

Chen JJ, Rosas HD, Salat DH, 2011. Age-associated reductions in cerebral blood flow are independent from regional atrophy. Neuroimage 55, 468–478. [PubMed: 21167947]

Cho J, Kee Y, Spincemaille P, Nguyen TD, Zhang J, Gupta A, Zhang S, Wang Y, 2018. Cerebral metabolic rate of oxygen (CMRO2) mapping by combining quantitative susceptibility mapping (QSM) and quantitative blood oxygenation level-dependent imaging (qBOLD). Magn. Reson. Med 80, 1595–1604. [PubMed: 29516537]

Fan AP, Bilgic B, Gagnon L, Witzel T, Bhat H, Rosen BR, Adalsteinsson E, 2014. Quantitative oxygenation venography from MRI phase. Magn. Reson. Med 72, 149–159. [PubMed: 24006229]

Fernandez-Miranda JC, de Oliveira E, Rubino PA, Wen HT, Rhoton AL Jr., 2010. Microvascular anatomy of the medial temporal region: part 1: its application to arteriovenous malformation surgery. Neurosurgery 67, 237–276 onsdiscussion ons276. [PubMed: 20539250]

Gur RC, Ragland JD, Reivich M, Greenberg JH, Alavi A, Gur RE, 2009. Regional differences in the coupling between resting cerebral blood flow and metabolism may indicate action preparedness as a default state. Cereb. Cortex 19, 375–382. [PubMed: 18534991]

Haacke EM, Tang J, Neelavalli J, Cheng YC, 2010. Susceptibility mapping as a means to visualize veins and quantify oxygen saturation. J. Magn. Reson. Imaging 32, 663–676. [PubMed: 20815065]

Hatazawa J, Fujita H, Kanno I, Satoh T, Iida H, Miura S, Murakami M, Okudera T, Inugami A, Ogawa T, et al. , 1995. Regional cerebral blood flow, blood volume, oxygen extraction fraction, and oxygen utilization rate in normal volunteers measured by the autoradiographic technique and the single breath inhalation method. Ann. Nucl. Med 9, 15–21. [PubMed: 7779525]

Hawkins WW, Speck E, Leonard VG, 1954. Variation of the hemoglobin level with age and sex. Blood 9, 999–1007. [PubMed: 13208753]

He X, Yablonskiy DA, 2007. Quantitative BOLD: mapping of human cerebral deoxygenated blood volume and oxygen extraction fraction: default state. Magn. Reson. Med 57, 115–126. [PubMed: 17191227]

Henriksen OM, Gjedde A, Vang K, Law I, Aanerud J, Rostrup E, 2021. Regional and interindividual relationships between cerebral perfusion and oxygen metabolism. J. Appl. Physiol 130, 1836–1847 (1985). [PubMed: 33830816]

Henriksen OM, Vestergaard MB, Lindberg U, Aachmann-Andersen NJ, Lisbjerg K, Christensen SJ, Rasmussen P, Olsen NV, Forman JL, Larsson HBW, Law I, 2018. Interindividual and regional relationship between cerebral blood flow and glucose metabolism in the resting brain. J. Appl. Physiol 125, 1080–1089 (1985). [PubMed: 29975605]

Hoge RD, Atkinson J, Gill B, Crelier GR, Marrett S, Pike GB, 1999. Investigation of BOLD signal dependence on cerebral blood flow and oxygen consumption: the deoxyhemoglobin dilution model. Magn. Reson. Med 42, 849–863. [PubMed: 10542343]

Ibaraki M, Miura S, Shimosegawa E, Sugawara S, Mizuta T, Ishikawa A, Amano M, 2008. Quantification of cerebral blood flow and oxygen metabolism with 3-dimensional PET and 15O: validation by comparison with 2-dimensional PET. J. Nucl. Med 49, 50–59. [PubMed: 18077532]

Ibaraki M, Sato K, Mizuta T, Kitamura K, Miura S, Sugawara S, Shinohara Y, Kinoshita T, 2009. Evaluation of dynamic row-action maximum likelihood algorithm reconstruction for quantitative 15O brain PET. Ann. Nucl. Med 23, 627–638. [PubMed: 19562437]

Ishii K, Kitagaki H, Kono M, Mori E, 1996. Decreased medial temporal oxygen metabolism in Alzheimer's disease shown by PET. J. Nucl. Med 37, 1159–1165. [PubMed: 8965188]

Jack CR Jr., Petersen RC, Xu YC, Waring SC, O'Brien PC, Tangalos EG, Smith GE, Ivnik RJ, Kokmen E, 1997. Medial temporal atrophy on MRI in normal aging and very mild Alzheimer's disease. Neurology 49, 786–794. [PubMed: 9305341]

Jain V, Langham MC, Wehrli FW, 2010. MRI estimation of global brain oxygen consumption rate. J. Cereb. Blood Flow Metab 30, 1598–1607. [PubMed: 20407465]

Jiang D, Deng S, Franklin CG, O'Boyle M, Zhang W, Heyl BL, Pan L, Jerabek PA, Fox PT, Lu H, 2021. Validation of T2 -based oxygen extraction fraction measurement with (15) O positron emission tomography. Magn. Reson. Med 85, 290–297. [PubMed: 32643207]

Jiang D, Lin Z, Liu P, Sur S, Xu C, Hazel K, Pottanat G, Darrow J, Pillai JJ, Yasar S, Rosenberg P, Moghekar A, Albert M, Lu H, 2020. Brain Oxygen Extraction Is Differentially Altered by Alzheimer's and Vascular Diseases. J. Magn. Reson. Imaging 52, 1829–1837. [PubMed: 32567195]

Jiang D, Liu P, Li Y, Mao D, Xu C, Lu H, 2018. Cross-vendor harmonization of T2 -relaxation-under-spin-tagging (TRUST) MRI for the assessment of cerebral venous oxygenation. Magn. Reson. Med 80, 1125–1131. [PubMed: 29369415]

Jiang D, Lu H, Parkinson C, Su P, Wei Z, Pan L, Tekes A, Huisman T, Golden WC, Liu P, 2019. Vessel-specific quantification of neonatal cerebral venous oxygenation. Magn. Reson. Med 82, 1129–1139. [PubMed: 31066104]

Krishnamurthy LC, Mao D, King KS, Lu H, 2016. Correction and optimization of a T2-based approach to map blood oxygenation in small cerebral veins. Magn. Reson. Med 75, 1100–1109. [PubMed: 25846113]

Lajoie I, Nugent S, Debacker C, Dyson K, Tancredi FB, Badhwar A, Belleville S, Deschaintre Y, Bellec P, Doyon J, Bocti C, Gauthier S, Arnold D, Kergoat MJ, Chertkow H, Monchi O, Hoge RD, 2017. Application of calibrated fMRI in Alzheimer's disease. Neuroimage Clin. 15, 348–358. [PubMed: 28560160]

Lin Z, Jiang D, Liu P, Ge Y, Moghekar A, Lu H, 2022. Blood-brain barrier permeability in response to caffeine challenge. Magn. Reson. Med 88, 2259–2266. [PubMed: 35754146]

Lin Z, Sur S, Soldan A, Pettigrew C, Miller M, Oishi K, Bilgel M, Moghekar A, Pillai JJ, Albert M, Lu H, 2019. Brain Oxygen Extraction by Using MRI in Older Individuals: Relationship to Apolipoprotein E Genotype and Amyloid Burden. Radiology 292, 140–148. [PubMed: 31012816]

Lipowsky HH, Usami S, Chien S, 1980. In vivo measurements of "apparent viscosity" and microvessel hematocrit in the mesentery of the cat. Microvasc. Res 19, 297–319. [PubMed: 7382851]

Lu H, Ge Y, 2008. Quantitative evaluation of oxygenation in venous vessels using T2-Relaxation-Under-Spin-Tagging MRI. Magn. Reson. Med 60, 357–363. [PubMed: 18666116]

Lu H, Xu F, Grgac K, Liu P, Qin Q, van Zijl P, 2012. Calibration and validation of TRUST MRI for the estimation of cerebral blood oxygenation. Magn. Reson. Med 67, 42–49. [PubMed: 21590721]

Lu H, Xu F, Rodrigue KM, Kennedy KM, Cheng Y, Flicker B, Hebrank AC, Uh J, Park DC, 2011. Alterations in cerebral metabolic rate and blood supply across the adult lifespan. Cereb. Cortex 21, 1426–1434. [PubMed: 21051551]

MacDonald ME, Frayne R, 2015. Phase contrast MR imaging measurements of blood flow in healthy human cerebral vessel segments. Physiol. Meas 36, 1517–1527. [PubMed: 26020543]

Mathew I, Gardin TM, Tandon N, Eack S, Francis AN, Seidman LJ, Clementz B, Pearlson GD, Sweeney JA, Tamminga CA, Keshavan MS, 2014. Medial temporal lobe structures and hippocampal subfields in psychotic disorders: findings from the Bipolar-Schizophrenia Network on Intermediate Phenotypes (B-SNIP) study. JAMA Psychiatry 71, 769–777. [PubMed: 24828364]

Mintun MA, Raichle ME, Martin WR, Herscovitch P, 1984. Brain oxygen utilization measured with O-15 radiotracers and positron emission tomography. J. Nucl. Med 25, 177–187. [PubMed: 6610032]

Mursch K, Wachter A, Radke K, Buhre W, Al-Sufi S, Munzel U, Behnke-Mursch J, Kolenda H, 2001. Blood flow velocities in the basal vein after subarachnoid haemorrhage. A prospective study using transcranial duplex sonography. Acta Neurochir. (Wien) 143, 793–799 discussion 799–800. [PubMed: 11678400]

Ohnishi T, Matsuda H, Hashimoto T, Kunihiro T, Nishikawa M, Uema T, Sasaki M, 2000. Abnormal regional cerebral blood flow in childhood autism. Brain 123 (9), 1838–1844 Pt. [PubMed: 10960047]

Peng SL, Dumas JA, Park DC, Liu P, Filbey FM, McAdams CJ, Pinkham AE, Adinoff B, Zhang R, Lu H, 2014. Age-related increase of resting metabolic rate in the human brain. Neuroimage 98, 176–183. [PubMed: 24814209]

Rhoton AL Jr., 2002. The cerebral veins. Neurosurgery 51, S159–S205.

Schuchardt F, Schroeder L, Anastasopoulos C, Markl M, Bäuerle J, Hennemuth A, Drexl J, Valdueza JM, Mader I, Harloff A, 2015. In vivo analysis of physiological 3D blood flow of cerebral veins. Eur. Radiol 25, 2371–2380. [PubMed: 25638218]

Thomas BP, Sheng M, Tseng BY, Tarumi T, Martin-Cook K, Womack KB, Cullum MC, Levine BD, Zhang R, Lu H, 2017. Reduced global brain metabolism but maintained vascular function in amnestic mild cognitive impairment. J. Cereb. Blood Flow Metab 37, 1508–1516. [PubMed: 27389176]

Tubbs RS, Loukas M, Louis RG Jr., Shoja MM, Askew CS, Phantana-Angkool A, Salter EG, Oakes WJ, 2007. Surgical anatomy and landmarks for the basal vein of rosenthal. J. Neurosurg 106, 900–902. [PubMed: 17542537]

van Zijl PC, Eleff SM, Ulatowski JA, Oja JM, Ulug AM, Traystman RJ, Kauppinen RA, 1998. Quantitative assessment of blood flow, blood volume and blood oxygenation effects in functional magnetic resonance imaging. Nat. Med 4, 159–167. [PubMed: 9461188]

Wise RG, Harris AD, Stone AJ, Murphy K, 2013. Measurement of OEF and absolute CMRO2: MRI-based methods using interleaved and combined hypercapnia and hyperoxia. Neuroimage 83, 135–147. [PubMed: 23769703]

Xu F, Liu P, Pekar JJ, Lu H, 2015. Does acute caffeine ingestion alter brain metabolism in young adults? Neuroimage 110, 39–47. [PubMed: 25644657]

Xu Y, Mohyeldin A, Nunez MA, Doniz-Gonzalez A, Vigo V, Cohen-Gadol AA, Fernandez-Miranda JC, 2021. Microvascular anatomy of the medial temporal region. J. Neurosurg 1–13.

Yamaguchi T, Kanno I, Uemura K, Shishido F, Inugami A, Ogawa T, Murakami M, Suzuki K, 1986. Reduction in regional cerebral metabolic rate of oxygen during human aging. Stroke 17, 1220–1228. [PubMed: 3492786]

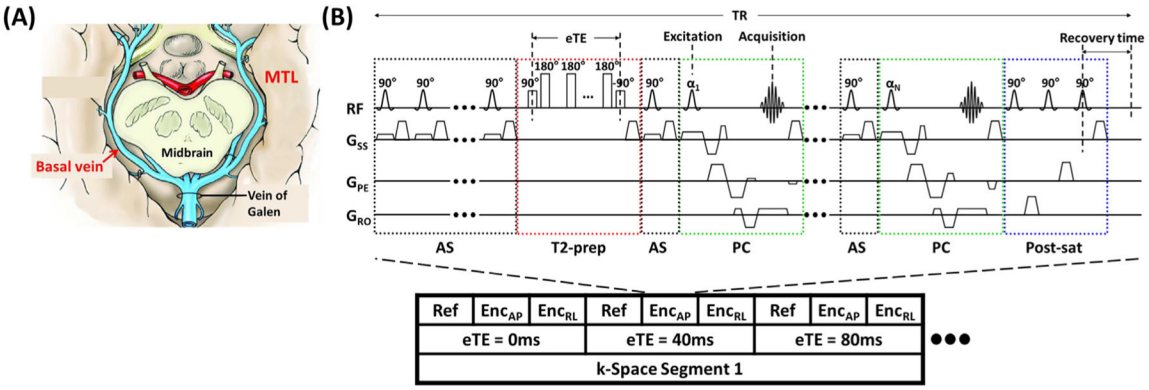

Fig. 1.

Illustration of venous drainage of deep brain tissues and diagram of the AS-aTRUPC sequence. (A) BVs run alongside the MTL and midbrain and drain into the vein of Galen, adapted from (Tubbs et al., 2007) with permission. (B) Sequence diagram of AS-aTRUPC. Three eTEs by T_2-preparation (T_2-prep, red box) are acquired in an interleaved fashion. At each eTE, one phase reference (Ref) image, one anterior-posterior flow-encoded image (Enc_{AP}) and one right-left flow-encoded image (Enc_{RL}) are acquired. A train of phase-contrast (PC, green boxes) modules are applied to acquire multiple *k* space lines per repetition time (TR). Arterial-suppression (AS) pulses (black boxes) are played before T_2-prep and before each excitation pulse. At the end of TR, post-saturation (post-sat, blue box) pulses reset magnetization to 0.

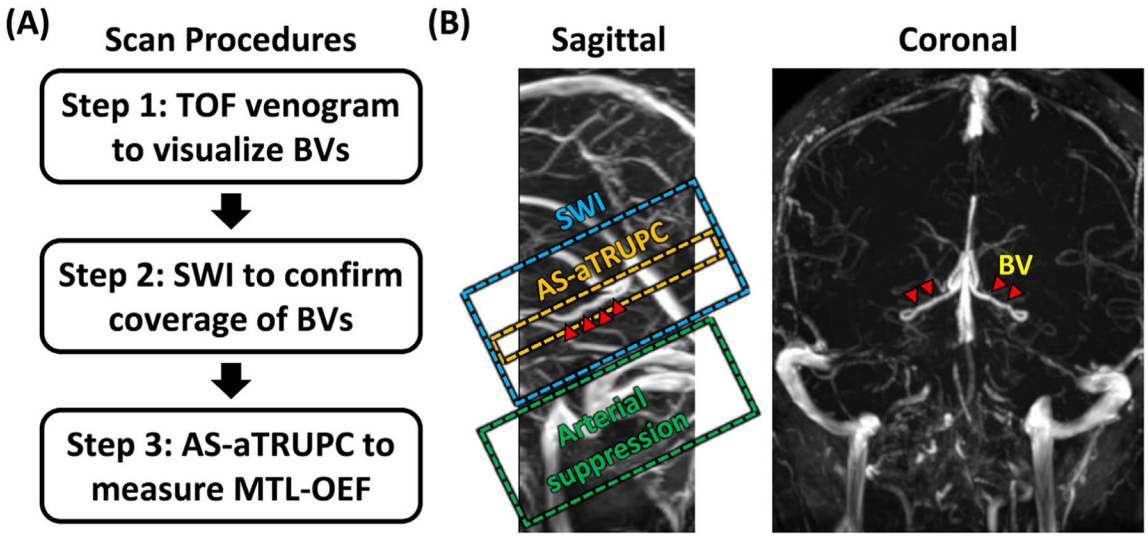

Fig. 2.

Scan procedures and positioning of pulse sequences. (A) Step-by-step scan procedures to measure MTL-OEF. (B) TOF maximum intensity projection images showing the BVs (red arrows). The positions of the SWI scan (blue box), the imaging slice (yellow box) and the arterial-suppression slab (green box) of AS-aTRUPC are shown in the sagittal TOF image.

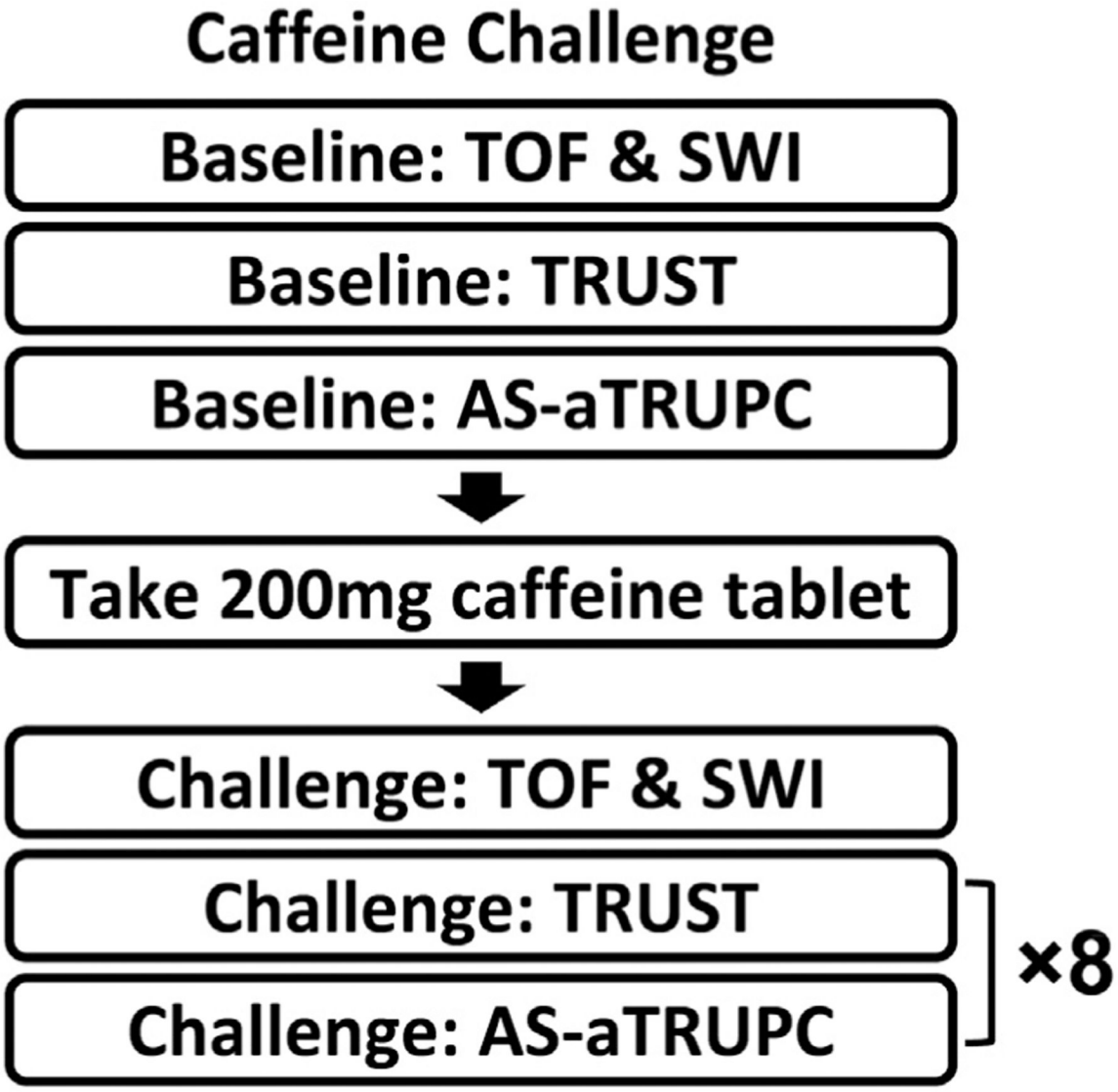

Fig. 3.
Experimental procedures of the caffeine challenge study. TOF and SWI were used to position the AS-aTRUPC scans at baseline and after caffeine ingestion.

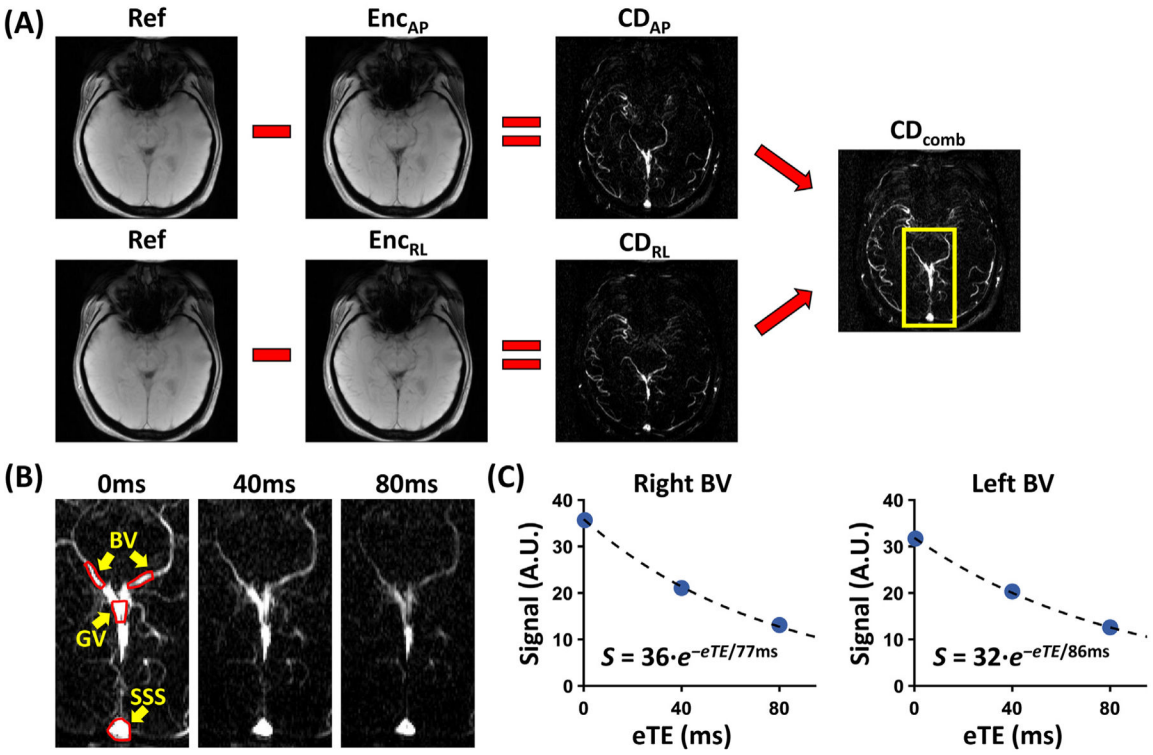

Fig. 4.

Representative AS-aTRUPC data. (A) Phase reference (Ref), anterior-posterior flow-encoded (Enc_{AP}), right-left flow-encoded (Enc_{RL}) images, and CD images along the two flow-encoding directions (CD_{AP} and CD_{RL}), as well as the combined CD image (CD_{comb}) are shown for eTE = 0ms. (B) Zoom-in views of the combined CD images (yellow box in A) for all eTEs. The red contours represent the ROIs for quantitative analyses. (C) Averaged signal intensities in the two BV ROIs as functions of eTEs. The fitted equations are also shown.

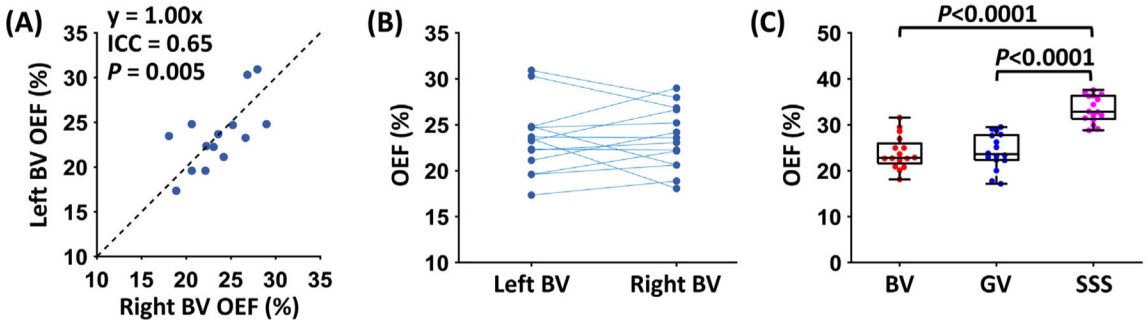

Fig. 5.

MTL-OEF in healthy adults. (A) Scatter plot showing significant linear correlation (ICC = 0.65, $P = 0.005$) between left and right BV OEF values. The dashed line represents the unit line. (B) Paired dot plot showing no difference between left and right BV OEF values (paired t-test $P = 0.94$). Dots from the same subject are connected by a solid line. (C) Comparison of OEF in BV, GV and SSS across the subjects. Median, interquartile range, minimum and maximum of the data points are shown in the box plots.

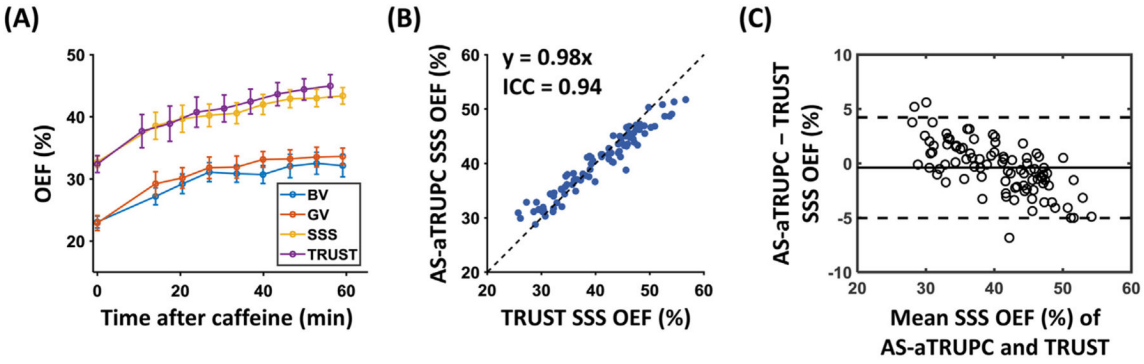

Fig. 6.

Results of the caffeine challenge study. (A) OEF at baseline (Time = 0) and after caffeine ingestion. Error bars represent standard errors of the OEF values across the subjects at each time point. (B) Scatter plot between OEF in the SSS measured by AS-aTRUPC and TRUST. The dashed line represents the unit line. (C) Bland-Altman plot comparing OEF in the SSS measured by AS-aTRUPC and TRUST. The solid line represents the mean OEF difference, and the dashed lines indicate the 95% confidence interval.

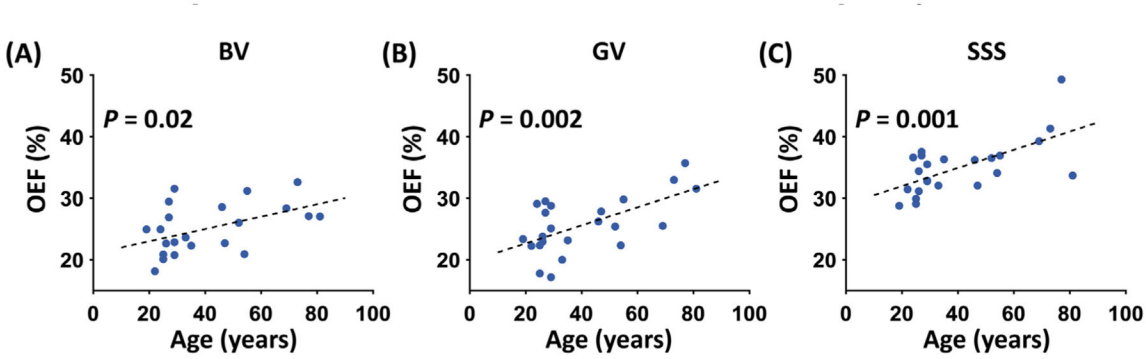

Fig. 7.

Age effect on OEF. Scatter plots between age and OEF in (A) BV, (B) GV, and (C) SSS measured by AS-aTRUPC.

Table 1

Results of OEF changes following caffeine ingestion. Three veins measured by AS-aTRUPC MRI were investigated. For each vein, the linear and quadratic changes in OEF were examined.

Model	Dependent variable	Independent variables	Coefficient	Standard Error	*P*-value
1	OEF in BV	Time	0.144%/min	0.016%/min	<0.0001
2	OEF in BV	Time	0.349%/min	0.052%/min	<0.0001
		$Time^2$	$-0.003\%/min^2$	$0.001\%/min^2$	< 0.0001
3	OEF in GV	Time	0.161%/min	0.017%/min	< 0.0001
4	OEF in GV	Time	0.408%/min	0.053%/min	< 0.0001
		$Time^2$	$-0.004\%/min^2$	$0.001\%/min^2$	< 0.0001
5	OEF in SSS	Time	0.161%/min	0.016%/min	< 0.0001
6	OEF in SSS	Time	0.338%/min	0.052%/min	< 0.0001
		$Time^2$	$-0.003\%/min^2$	$0.001\%/min^2$	0.0006

Note: OEF = oxygen extraction fraction, AS-aTRUPC = arterial-suppressed accelerated T_2-relaxation-under-phase-contrast, BV = basal vein of Rosenthal, GV = vein of Galen, SSS = superior sagittal sinus.

Table 2

Association of OEF with age. Three veins measured by AS-aTRUPC MRI were examined separately.

Model	Dependent variable	Independent variables	Coefficient	Standard Error	*P*-value
1	OEF in BV	Age	0.100%/year	0.039%/year	0.02
2	OEF in GV	Age	0.146%/year	0.041%/year	0.002
	OEF in SSS	Age	0.148%/year	0.039%/year	0.001

Note: OEF = oxygen extraction fraction, AS-aTRUPC = arterial-suppressed accelerated T_2-relaxation-under-phase-contrast, BV = basal vein of Rosenthal, GV = vein of Galen, SSS = superior sagittal sinus.